Physics of Fluids

Self-generated electrostatic forces of drops rebounding from hydrophobic surfaces

Cite as: Phys. Fluids **35**, 017111 (2023); https://doi.org/10.1063/5.0130343
Submitted: 11 October 2022 • Accepted: 11 December 2022 • Published Online: 04 January 2023

Diego Díaz, Xiaomei Li, Pravash Bista, et al.

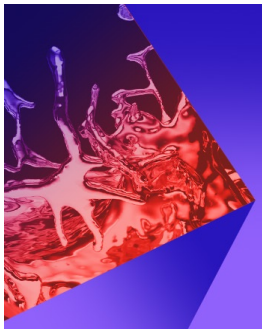

Physics of Fluids ARTICLE scitation.org/journal/phf

Self-generated electrostatic forces of drops rebounding from hydrophobic surfaces

Cite as: Phys. Fluids **35**, 017111 (2023); doi: 10.1063/5.0130343
Submitted: 11 October 2022 · Accepted: 11 December 2022 ·
Published Online: 4 January 2023

Diego Díaz, Xiaomei Li, Pravash Bista, Xiaoteng Zhou, Fahimeh Darvish, Hans-Jürgen Butt,[a] and Michael Kappl[a]

AFFILIATIONS

Max Planck Institute for Polymer Research, Ackermannweg 10, 55128 Mainz, Germany

[a]Authors to whom correspondence should be addressed: butt@mpip-mainz.mpg.de and kappl@mpip-mainz.mpg.de

ABSTRACT

We study the charge separation of drops rebounding from hydrophobic surfaces. Based on high-speed video imaging and the deflection of drops by electric fields, we reproducibly detected the amount of charge. Here, we show that the charge separation of bouncing drops can be 2 orders of magnitude higher on hydrophobic than superhydrophobic surfaces. We observed the existence of self-generated electrostatic forces between the drop and the surface. These forces affect the maximum rebounding height and slow down the retraction motion of drops. We additionally calculated the electrostatic forces using an energy conservation approach. Our results indicate that electrostatic forces on hydrophobic surfaces can be even stronger than gravity, reducing the restitution coefficients up to 50%. This new approach becomes advantageous compared with other methods that require more complicated setups for drop charge detection.

I. INTRODUCTION

When water drops move in contact with hydrophobic surfaces, charge separation occurs at the moving three-phase contact line. Examples range from drops sliding on tilted hydrophobic surfaces,[1–5] drops that coalesce and then jump positively charged,[6] up to drops impacting and rebounding off of solid surfaces. Usually, water drops charge positively and leave the surface with the opposite net charge.[7–12]

The charge transfer mechanism has been explained as a contribution of both ion[13–16] and electron transfer[17] at the liquid–solid interface. The formation of an electrical double layer and its subsequent disruption would be responsible for breaking the electroneutrality at the solid–liquid interface. Charge separation has attracted both fundamental and applied interest. From a fundamental motivation, charging can affect the dynamic wetting of surfaces.[18–20] In fact, even electrostatic forces generate between a sliding drop and a hydrophobic surface.[21] These forces influence the speed of sliding drops, as they can even exceed gravitational force. In terms of applications, charge separation has been demonstrated to allow the conversion of kinetic energy to electric energy.[11,22–34]

Recently, we showed that water drops acquire a positive net charge after rebounding from superhydrophobic surfaces. The amount of charge mainly depends on the maximum drop contact area.[12] As the drop retracts, charge separation occurs, and drops continuously gain a positive charge while depositing the opposite net charge on the surface. This phenomenon can be described quantitatively by a model developed for charging of sliding drops.[5] This model considers drops as a capacitor that stores charge up to a saturation point. However, the amount of charge coming from superhydrophobic surfaces is much less than the hydrophobic ones. For that reason, energy-harvesting applications have focused mainly on drops sliding on hydrophobic coatings to improve the efficiency. Furthermore, it is difficult to find a hydrophobic surface with sufficient repellency to produce complete rebounds. As a result, charge separation by drop impact on these surfaces has not been widely studied. One suitable surface is Teflon AF, which has been used for drop impact[35] and slide electrification experiments[21] due to its high hydrophobicity. More insight on these surfaces could allow us to describe charge separation under different drop impact dynamics and wetting states.

The outcomes of drop impact on hydrophobic surfaces have been studied before.[36–41] Usually, the energy balance of bouncing drops is described by different sources such as the surface energy, viscous dissipation, gravitation, and kinetic energy.[42–47] However, the influence of charging in the drop impact dynamics has never been considered. Here, we show that impacting water drops on Teflon AF surfaces can also be considerably influenced by self-generated electrostatic Coulomb forces. These forces are generated by spontaneous

drop charging, which can evidently affect the retraction motion and the maximum rebounding height. We quantify the charge using a homogeneous lateral electric field and high-speed video imaging.

II. MATERIALS AND METHODS

A. Sample preparation

For our drop impact experiments, we used two types of surfaces: Teflon AF1600 as hydrophobic surface and SU-8 micropillar array as a hydrophobic surface that behaves almost as superhydrophobic (Cassie state of rebounding drops). We performed experiments up to impact speeds of 1.73 m/s for Teflon AF1600 and up to 0.77 m/s in the case of micropillars.

1. Teflon AF1600

Teflon AF1600 (Teflon) films were prepared by dip coating of $75 \times 25\,\text{mm}^2$ slides of 1 mm thick SiO_2 and glass slides sputter-coated with a 30 nm gold layer. Before sputtering, glass slides were pre-coated with 5 nm chromium for adhesion improvement. Both SiO_2 slides and the gold-coated glass slides were immersed into 1 wt. % Teflon AF1600 (Sigma Aldrich) in FC-317 43 (Sigma Aldrich) with a speed of 90 mm/min. After being immersed for 10 s, the substrates were withdrawn from the solution at a constant speed of 10 mm/min. Finally, the films on the substrates were annealed at 160 °C in a vacuum for 24 h. Teflon AF1600 films were 60 nm thick with a roughness $\leq$1 nm according to scanning force microscopy measurements over an area $0.5 \times 0.5\ \mu\text{m}^2$ [Fig. 1(a)]. Teflon AF1600 on gold and SiO_2 showed practically the same wetting properties, with contact angle hysteresis of $13° \pm 3°$ and $12° \pm 3°$, respectively, and a static contact angle of $120° \pm 2°$. As a result, Teflon AF1600 showed sufficient hydrophobicity to let the drops rebound completely from the surface. Here, we refer to a "complete rebound" when drops rebound off of the surface without leaving a part of the total liquid volume stick on the surface [Fig. 1(b) (Multimedia view)]. On the other hand, we called "partial rebound" when the liquid volume not attached to the surface is the one that rebounds (Fig. S1). It should be noted, at this point, that we had also tried to use other hydrophobic surfaces such as silicon wafers and glass surfaces that were hydrophobized with perfluorosilanes. For all these surfaces, we encountered the problem that drops rebound partially or not fully vertical even in the absence of the electric field. We attribute the lateral motion after a rebound to subtle differences in local contact angle or slight contact line pinning that leads to lateral force components at the contact line during drop rebound.

2. SU-8 micropillar arrays surfaces

As substrates, we used 1 mm thick, rectangular glass slides of $75 \times 25\,\text{mm}^2$. First, two cycles (15 min) of ultrasonication with

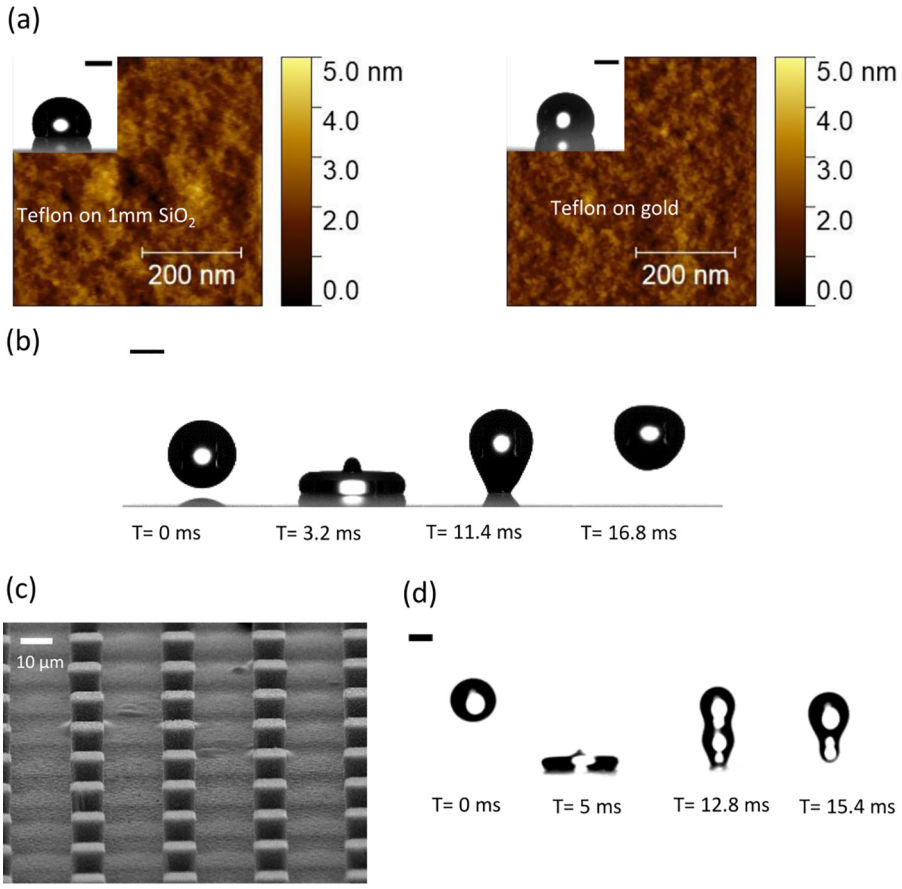

FIG. 1. (a) AFM tapping mode images of Teflon films on bare (left) and gold-coated (right) SiO_2 slides. (b) High-speed video images of a 4 μL drop rebounding from Teflon-SiO_2 (impact speed, $v_0 = 0.5$ m/s). (c) Scanning electron microscopy image of a rectangular-shaped micropillar surface. (d) High-speed video images of a 4 μL drop rebounding from a SU-8 micropillar surface ($v_0 = 0.6$ m/s). Scale bars represent 1 mm. Multimedia views: https://doi.org/10.1063/5.0130343.1; https://doi.org/10.1063/5.0130343.2

acetone were done to remove organic contaminants, followed by 2-propanol (15 min) which removes acetone's contaminated residues. Afterward, substrates were dry blown using a filtered nitrogen gun. Then, 1 ml of SU-8 was dropped on the clean glass. A two-step spin coating process was carried out (step 1: 5 s, 500 rpm, with 200 rpm^{-1} acceleration, step 2: 30 s, 3000 rpm, with 200 $rpms^{-1}$ acceleration). To degass SU-8 to avoid bubble formation, the SU-8 samples were put into a vacuum. The soft baking process was carried out on a hotplate at 65 and 95 °C for 70 min. After cooling down to room temperature, a photomask (rectangular patterns of 10×5 μm^2, spacing 20 μm [Fig. 1(c) and S2] was placed on top of the sample and it was exposed to I-line UV light for 8 s. Finally, they were developed for 3 min with the SU-8 developer and washed with 2-propanol for 1 min. The resulting surfaces of rectangular-shaped micropillars with a spacing distance of 20 and 10 mm height were hydrophobic with a static contact angle of $\theta_s = 133° \pm 3°$ and hysteresis of $20° \pm 2°$. Drops showed complete rebounds for impact heights between 0.5 and 3 cm [Fig. 1(d) (Multimedia view)]. Thus, drops remain in the Cassie Baxter state[48] during the impact.

B. Experimental setup

We used the electric field method reported in our previous work[12] for drop charge detection. About 4 μL drops were released from a grounded motorized syringe pump from 1 to 15 cm height (impact speed $v_0 = 1, \ldots, 1.7$ m/s) onto hydrophobic sample surfaces. The impact speed was calculated by the expression $v_0 = \sqrt{2gH}$, where g is the gravity acceleration and H is the release height of drops. After dispensing the drops, using two copper plates ($50 \times 16 \times 4$ mm^3), we simultaneously applied a lateral electric field of $E = U/d = 50, \ldots,$ 100 kV [Fig. 2(a)], where U is the applied voltage (Analogic AN-3200) and d is the separation distance of the plates. Both copper plates were vertically placed over a Teflon plate that works as an insulating support. We recorded the impact process by high-speed video imaging (Photron FastCam Mini UX100) at 5000 fps, to track trajectory of the drop mass center. The drop mass center was determined at each frame of the videos by a MATLAB algorithm.[12] We neutralized the surface using an ionizing air blower (Aerostat PC Ionizing Air Blower, PA) for 2 min before each drop impact. This ensures the electrical neutrality of the surface and drop (grounded syringe) prior to the impact. Here, we only focus on the impact of single drops because multiple consecutive drops lead to build up charge on the surface.[21] Before each drop impact, the surface charge is neutralized by the ionizing air blower and allows us to use a "fresh" surface and a "first drop" for each experiment. All the rebounding drops stayed below the upper end of the plates, so the electric field experienced by the drops can be assumed to be homogeneous. We shielded the syringe and drop with an aluminum tube to avoid polarization of drops. To calibrate the charge measurements, we used an electrode (50 μm thick tungsten wire) that touches the drop when falling down and after the rebound [Figs. 2(b)–2(d) (Multimedia view)]. This electrode detects a current signal during the contact with the drop. Integrating the current signal over time gives the total charge of the drop to compare. Drop charge values obtained by discharge via the electrode or deflection by the electric field were close to each other (Fig. S3). All the experiments were repeated four times and performed at a relative humidity of 30%–40%. At such low values of humidity, no influence of the humidity on the charging process is expected.[49]

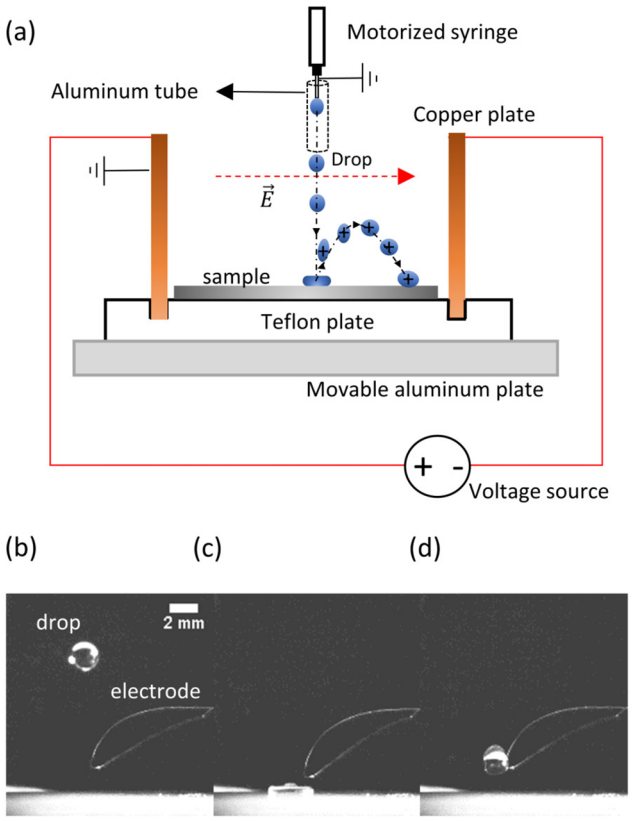

FIG. 2. (a) Schematic of the experimental setup of electric fields. [(b)–(d)] Calibration measurement of a drop impacting a Teflon on SiO_2 surface. Three moments are shown: (b) drop falling down, (c) drop impacting the surface, and (d) drop in contact with the probe after bouncing. Multimedia view: https://doi.org/10.1063/5.0130343.3

III. RESULTS AND DISCUSSION

A. Teflon on SiO_2

1. Drop charge detection

When a drop impacts the surface, the initial kinetic energy is converted gradually into surface energy until the drop reaches the maximum spreading diameter, D_{max}. Then, the surface tension forces lead to a retraction motion until the drop bounces off of the surface. After the taking off, drops are laterally deflected by an electrostatic force $F_E = QE$ (Q is drop charge) in the same direction of the external electric field [Figs. 3(a) and 3(b) (Multimedia view)]. Even secondary drops, that may be ejected from the top of the initial drop, so-called the Worthington jet,[50] are horizontally accelerated in the same direction. Thus, both primary and secondary drops carry a positive charge. The sign of the charge can be explained by the tendency of a surface coated with fluoropolymers to absorb hydroxyl ions from water.[13,14,16,51] These negative ions and the counter positive ions in water can form a neutral electrical double layer. The contact line motion of a drop should break the electrical equilibrium of the double layer until drops detach from the surface with the positive charge. This non-equilibrium process has been suggested also for sliding[5] and

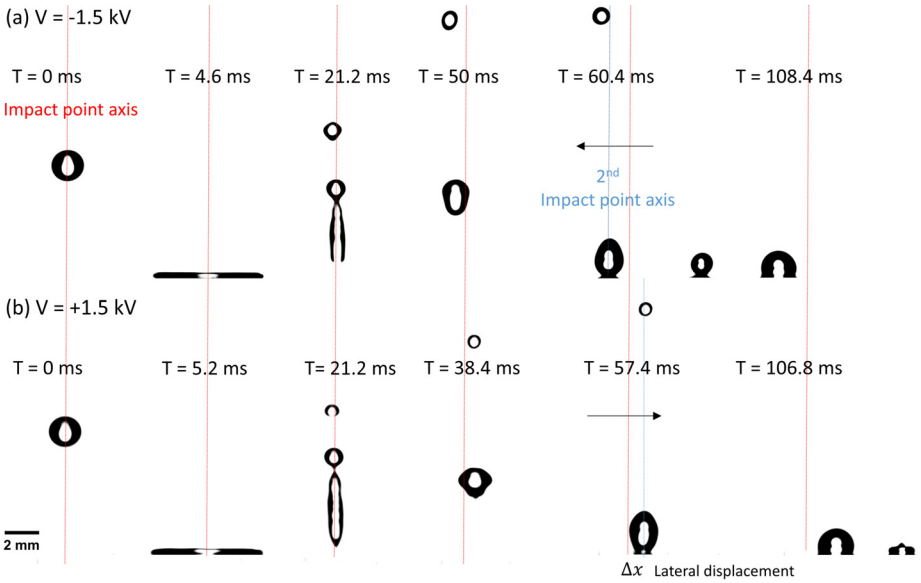

FIG. 3. Drops rebounding from Teflon AF films on SiO_2 and deflected by an applied electric field: (a) from right to left and (b) from left to right. Red and blue dotted lines represent the vertical axis at which the drop mass center was located during the impact and the second contact with the surface, respectively. Multimedia view: https://doi.org/10.1063/5.0130343.4

jumping drops[6] on surfaces coated with fluoropolymer like the coating of our substrates. Therefore, the same mechanism should be responsible for our positive rebounding drops.

Since drops after rebound move laterally with a constant acceleration, we can calculate the drop charge as follows:[12]

$$Q = \frac{2\rho V \Delta x}{Et^2}. \tag{1}$$

Here, ρ is the density of the liquid; V is the drop volume; Δx is the horizontal displacement of the drop mass center, from the taking off until the second contact with the surface; and t is the time lapse between the two contacts.

Drop charging on Teflon surfaces was only observed for impact speeds above 1.2 m/s, in the regime where a Worthington jet is generated.[50] This jet is a result of the collapse of an air cavity formed at the drop as it hits the surface.[52] Since both primary and secondary drops were deflected by the applied electric field, it is necessary to know their volume to calculate the drop charge. We calculated the volume of the ejected drop by its lateral and vertical diameters, assuming a spheroidal shape (Fig. S4). Uncertainty in measuring the drop volume is ∼8% (see the supplementary material, Sec. VII). Subtracting the ejected drop volume from the initial 4 μL drop, we obtain the primary drop volume. Thus, the total charge acquired by our drops is the sum of the charge of primary and secondary drops.

2. Influence of the Weber number

We represent the different impact speeds of our experiments in terms of the Weber number $We = \rho v_0^2 R_0/\gamma$, with R_0 as the initial drop radius, and γ as the surface tension. Uncertainty in We was up to ∼0.6 (see the supplementary material, Sec. VII). Above $We = 20$, we clearly observed the jetting. Below $We = 40$, the rebounding height and, therefore, the length of the drop trajectory are not sufficient to detect a significant deflection of drops. For $We > 40$, we observed an evident drop charging by using our electric field method. The volumes of secondary drops were between 0.35 and 1.55 μL, and their charge values ranged from 9 to 40 pC (Fig. S5). In addition, we observed that the secondary drop charge tends to increase with the volume, as expected by Eq. (1).

We have shown in our previous work[12] that the amount of charge of drops after taking off is a function of the maximum contact area $A_{max} = \pi R_{max}^2$ (R_{max} is the maximum contact radius, assuming a circular pattern)

$$Q(A_{max}) = -2\pi\sigma_S^0\lambda_r^2\left[1 - \exp\left(\frac{-(A_{max} - A_0)}{2\pi\lambda_r^2}\right)\right], \tag{2}$$

where σ_S^0 is the surface charge density at zero potential, reached its maximum spreading. λ_r is the radial decay length. This equation considers that σ_S^0 is maximum at the moment of full spreading. As the drop retracts, charge separation occurs and the negative charge is deposited on the surface most likely due to the deposition of hydroxyl ions. This leads to an increasing accumulation of positive charge in the drop, while it recoils. Then, the drop rebounds positively charged leaving a negatively charged area on the surface. As the drop is assumed to behave like a capacitor, it will store charge up to a saturation point at certain A_{max}. This saturation is set by λ_r, which is characteristic for each surface. After the saturation point, further spreading will not lead to an increment in charge. Consequently, if A_{max} is large enough, the charge left on the surface will be accumulated in an outer ring of the wetted area.

As A_{max} is determined by the impact speeds, it can be scaled with We. Plotting R_{max}/R_0 as a function of We leads to the scaling law $R_{max} \propto R_0 \mathrm{We}^{0.3}$ [Fig. 4(a)] and, thus, $A_{max} \propto \pi R_0^2 We^{0.6}$. Accordingly, we can express the drop charge as a function of We as follows:

$$Q(We) = -2\pi\sigma_S^0\lambda_r^2\left[1 - \exp\left(\frac{-\pi R_0^2(We^{0.6} - We_0^{0.6})}{2\pi\lambda_r^2}\right)\right], \tag{3}$$

where We_0 is the minimum Weber number at which the drop rebounds completely from the surface. It is important to mention that,

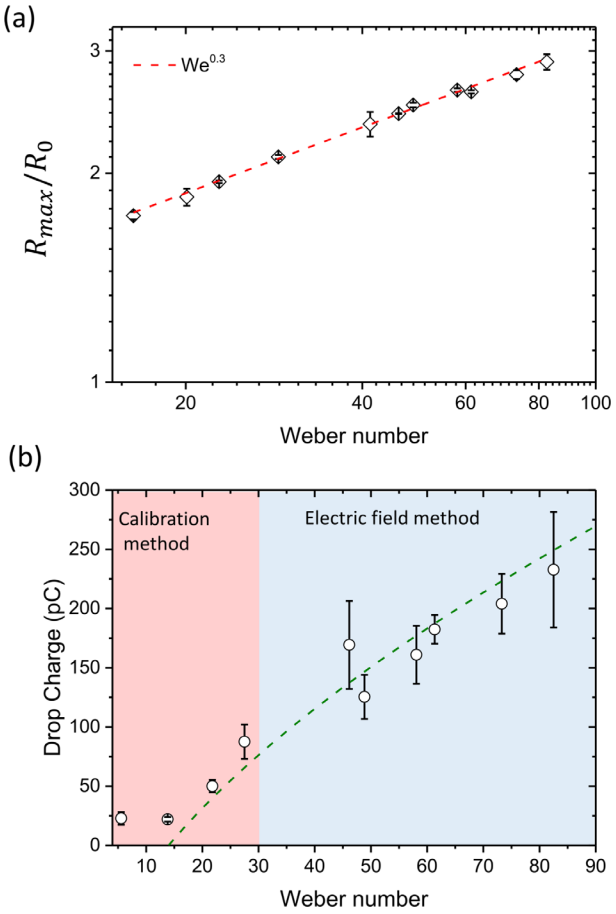

FIG. 4. (a) Spreading factor R_{max}/R_0 vs Weber number for Teflon SiO_2. The red dashed line represents the fit of $We^{0.3}$. (b) Drop charge vs Weber number for Teflon on SiO_2. Red shaded region encloses the data measured by the calibration method, whereas the blue one by the electric field method. The green dashed line represents the theoretical prediction in terms of the Weber number. The data include the charge of the primary and secondary drop for each Weber number. Error bars represent the standard deviation of four measurements.

by considering energy balance only between kinetic impact energy and surface energy at the moment of maximum spreading,[39,42] one obtains $R_{max} \propto R_0 \mathrm{We}^{1/2}$. This means that the initial kinetic energy of a drop right before impact is dissipated in other forms of energy during the spreading phase. Such sources of dissipation are suggested to be viscous dissipation[47] and internal fluid motion.[39] Moreover, the same power law for our Teflon surfaces was observed even for experiments in the absence of an applied electric field (Fig. S6). Thus, we can confirm that the applied electric fields do not lead to additional energy dissipation of our impacting drops.

Our experiments reveal that drop charge increases with *We* [Fig. 4(b)]. Note that in Fig. 4(b), since we cannot measure the drop charge for $We < 40$ by our electric field method, we added data points obtained from our calibration measurements with the wire electrode for $We < 30$. At this range, the drop charge decreases when decreasing *We* until reaching the lowest value from $We = 14$. The detection limit of our calibration setup is below $We = 5$, where drops do not rebound. We then chose $We_0 = 14$ as the moment where charging is minimum. Remarkedly, charge values on Teflon on SiO_2 can be more than six times higher than the values reported on superhydrophobic surfaces.[12] As the surface chemistry of the fluorinated superhydrophobic surfaces is not very different from that of Teflon, we attribute this much higher charging to the difference in the true contact area. Bouncing drops on superhydrophobic surfaces remain in the Cassie state, so the contact area distributes between the air entrapped in the surface and the solid surface itself. Therefore, as the hydrophobic Teflon on SiO_2 is flat and homogeneous, the true liquid–solid contact area will be larger, leading to more efficient charge separation.

Fitting Eq. (3) to the observed drop charge values [Fig. 4(b)], we found $\sigma_S^0 = 8.6\ \mu\mathrm{C/m^2}$ and $\lambda_r = 32\ \mathrm{mm}$, which is in good agreement with the values found by Li *et al.*[21] for water drops sliding on Teflon. This means that our electric field method is suitable to obtain the independent parameters σ_0 and λ_r for surfaces with sufficiently low wettability to allow complete rebounds, such as hydrophobic or superhydrophobic surfaces.

3. Teflon on gold

When the Teflon film was deposited on top of a thin conductive gold layer, no significant deflection of drops by the electric field could be detected. We can, therefore, conclude that charging can be reduced significantly by using conductive and high-permittivity substrates. This is compatible with experiments of sliding drops on the same surfaces, where charge values were ten times lower when conductive substrates were used.[21] In Sec. III B, we will describe and explain the implications of charging on the drop impact dynamics, specifically, in the energy dissipation at the retraction phase and after rebound.

B. Effects of electrostatic forces on drop kinetics

1. Retardation of the retraction motion

To elucidate the influence of charging on the drop impact dynamics, we measured the average spreading speed $\bar{V}_s = R_{max}/t_s$ and the average retraction speed $\bar{V}_r = R_{max}/t_r$ of our drops on Teflon. Here, t_s is the spreading time, i.e., the time lapse from the initial touching of the surface on the surface until the drop reaches R_{max}. t_r is the duration of the entire retraction phase until the drop rebounds. Both $\bar{V}_{ret}$ and $\bar{V}_s$ increase with *We* for our Teflon surfaces. However, $\bar{V}_s$ is practically identical for both Teflon surfaces [Fig. 5(a)], whereas $\bar{V}_r$ is higher for Teflon on gold than for Teflon on SiO_2, for $We > 10$ [Fig. 5(b)]. This suggests that charge separation occurs during the retraction phase as proposed in our previous work.[12] The observed retardation of the retraction motion is then caused by the self-generated electrostatic forces between the charged drop and the charge deposited on the surface. This means that below $We = 10$, charging is not sufficient to affect the drop retraction dynamics.

The full process of charging and retardation would be the following: As the drop spreads on the surface, an electrical double layer forms [Fig. 5(c)]. The formation of the double layer is estimated to be in 6 μs, which is much faster than the spreading of our drops (<3 ms).[5] When drops start to recede, part of the negative surface charges stay on the surface. The positive counter charges of the diffuse double layer remain in the drop. As a result, the drop is positively charged during the retraction and deposits the negative charge on the

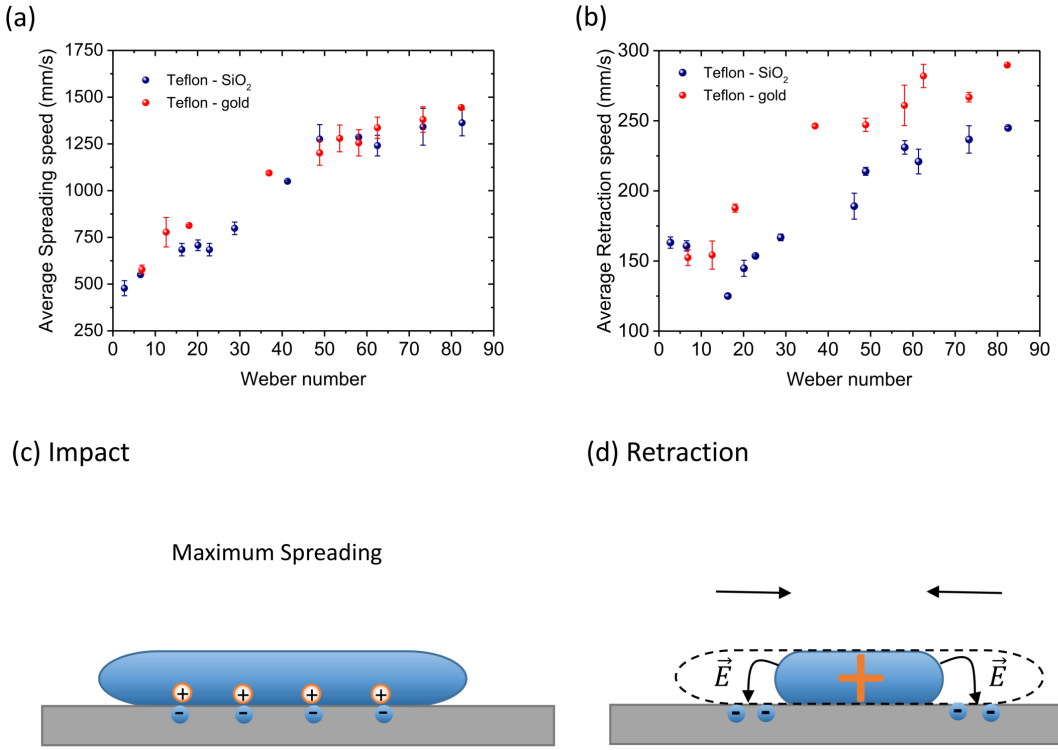

FIG. 5. (a) Average spreading speed vs Weber number of drops rebounding from Teflon on SiO_2. (b) Average retraction speed vs Weber number. (c) Schematic of the drop reaching the maximum spreading radius. (d) Schematic of the electrostatic forces acting on a positive retracting drop.

surface. This negative charge will attract the positive drop rim, slowing down its retraction [Fig. 5(d)]. Therefore, the retardation of the retraction motion is our first indicator that electrostatic forces affect the drop dynamics.

2. Reduction of the maximum rebounding height

If self-generated electrostatic forces affect the retraction phase, they should also influence the drop motion after rebound. For this reason, we compared the maximum rebounding height h_{max} of drops at different We on the two different Teflon substrates. Here, h_{max} is the maximum vertical position of the drop mass center, which was measured from the surface at $y = 0$. From the measurements of h_{max}, we observed that drops rebound higher for Teflon on gold than on SiO_2 [Fig. 6(a)], with a difference of up to a 45%. This means that no metallic substrates dissipate more energy as shown in the values of restitution coefficient $e = |v_0/v_1|$, where v_1 is the velocity at the moment of rebound [Fig. 6(b)]. Indeed, values of e are reduced up to 50% for Teflon on SiO_2 compared to Teflon on gold.

One possible source of energy dissipation after taking off is viscous damping, which is difficult to estimate precisely.[53] If viscous dissipation in air were the dominant source of energy loss, then drops rebounding from both Teflon substrates should reach similar h_{max}. However, this is not what we see experimentally. This suggests that electrostatic forces induced by charging are the main responsible for the variation of h_{max}. Hence, the reduction in h_{max} is our second indicator of electrostatic forces influencing the drop motion.

In this case, the reduction of h_{max} is due to the negative charges left on the surface once the drop rebounds positively charged from Teflon on SiO_2. These charges will lead to an electrostatic force, which retards the drop [Fig. 6(c)]. Accordingly, the rebounding drop will be decelerated by both electrostatic force and gravity.

C. Calculation of the electrostatic force

So far, we have shown the influence of electrostatic forces in the drop motion, specifically, during drop retraction and after rebound. In this section, we will calculate the electrostatic forces in both phases, based on an energy conservation approach.

1. Retraction motion

We first start with drops rebounding from Teflon-on-gold, that is, with no significant electrostatic component. The kinetic energy of drops before impact is given by

$$E_T = mgh_0 = \frac{1}{2}mv_0^2, \tag{4}$$

where m is the drop mass and h_0 is the falling height. At the moment of taking off, the energy is

$$E_R = \frac{1}{2}m_p v_{1p}^2 + \frac{1}{2}m_s v_{1s}^2 + m_p g h_{1p} + m_s g h_{1s}. \tag{5}$$

Here, the index "p" and "s" refer to the primary and secondary drops, respectively. This equation basically combines the kinetic and

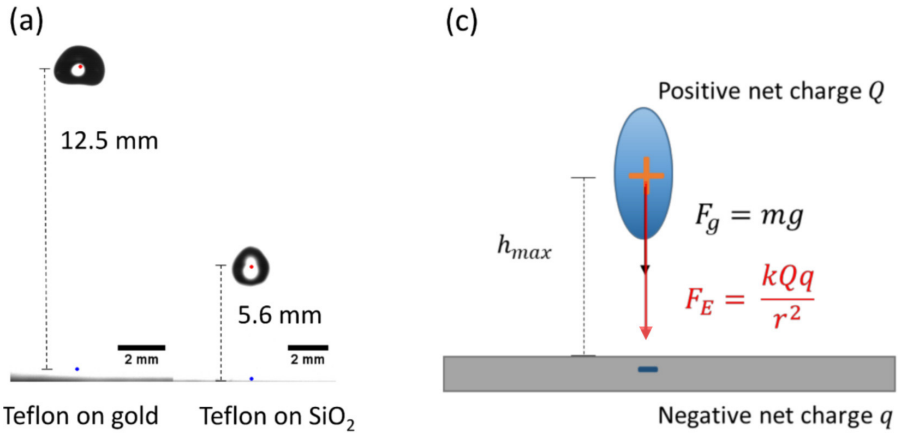

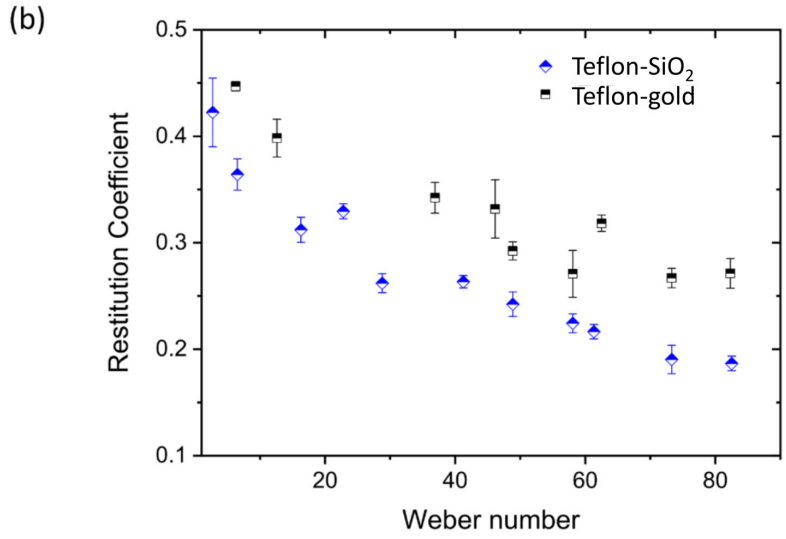

FIG. 6. (a) Drops reaching the maximum rebounding height for a Teflon on gold and SiO_2 ($We = 82$). Red points represent the position of the drop mass center when the drop reaches the maximum rebounding height. Blue points represent the position of the surface. (b) Restitution coefficient vs Weber number for Teflon surfaces. (c) Schematic of the electrostatic force acting on a rebounding drop.

potential energy of all the drops deflected by the electric field. h_1 and v_1 represent the height and speed after taking off, respectively. The vertical speed of drops was determined by the derivative of the vertical position of the drop mass center ($\frac{dy_{cm}}{dt}$). For drops rebounding from Teflon on SiO_2, we should add in Eq. (5) the electric energy acquired by drops due to charging

$$E_R = \frac{1}{2}m_p v_{1p}^2 + \frac{1}{2}m_s v_{1s}^2 + m_p g h_{1p} + \frac{Q_p^2}{4\pi\varepsilon_0 h_{1p}} + m_s g h_{1s} + \frac{Q_s^2}{4\pi\varepsilon_0 h_{1s}} + \frac{Q_p Q_s}{4\pi\varepsilon_0 (h_{1p} - h_{1s})}, \quad (6)$$

where ε_0 is the vacuum permittivity. The fourth and sixth terms are the electric energy of a primary (E_{Q1p}) and secondary drop (E_{Q1s}), respectively, at the moment of rebound. Note that, here, we assume that the net charge deposited on the surface is equivalent to the drop charge. The electric energy due to the electrostatic interaction between the primary and secondary drops (last term) is mostly in the order of 10^{-9} J, considering the small charge of secondary drops. This is two orders of magnitude smaller than the values of the kinetic energy of drops after rebound so that its contribution is not significant. The difference between E_T and E_R is the energy dissipated by hydrodynamic viscous dissipation, E_V, and by contact line friction, E_F, plus the work done by the electrostatic force required to retract the contact line against electrostatic forces, E_{ef}:

$$E_T - E_R = E_V + E_F + E_{ef}. \quad (7)$$

Here, $E_F = \pi\gamma(\cos\theta_r - \cos\theta_a)R_{max}^2$,[47] with θ_r and θ_a as the dynamic receding and advancing contact angles, respectively. In particular, for Teflon on SiO_2, $\theta_r = 120° \pm 2°$ and $\theta_a = 128° \pm 2°$. These angles were obtained from drops sliding down on the Teflon surface at different velocities. We used the same method of high-speed video processing reported by our group[54] to determine the dynamic contact angles.

E_V comes from the energy loss due to the motion of drops against viscous forces and occurs in a shear thin boundary layer at the

solid–liquid interface.[55,56] This means that E_V will depend on the velocity of the boundary flow. Considering the impact speed v_0 as the characteristic velocity of the boundary flow, E_V of an impacting drop can be approximated to the expression[47]

$$E_V = E_{V-S} + E_{V-R} \approx \frac{\mu B v_0^2 \tau_s R_{max}^2}{L_V} + \frac{\mu B V_0^2 \tau_r R_{max}^2}{L_V}, \quad (8)$$

where the energy loss in the spreading and retraction phase is represented by E_{V-S} and E_{V-R}, respectively. μ is the viscosity of the liquid, L_v is the characteristic dissipation length scale, and B is another constant. Using the definition of the average spreading speed and the average retraction speed, Eq. (8) yields

$$E_V = E_{V-S} + E_{V-R} \approx \alpha(\tau_s^3 \bar{V}_s^2 + \tau_r^3 \bar{V}_r^2) \quad (9)$$

with $\alpha = \mu B v_0^2 / L_v$. As both Teflon substrates exhibited for $We > 40$ practically the same values of $\bar{V}_s$ and t_s [Fig. S7(a)], their values of E_{V-S} should be equivalent at this range. Furthermore, t_r for Teflon on SiO_2 is up to a 18% higher than the retraction time for Teflon on gold at the same We [Fig. S7(b)], while $\bar{V}_r$ is up to 20% lower. This leads to a maximum difference of ~5% in E_{V-R} between the different Teflon substrates. As a result, for both types of surfaces, we can safely assume the same E_V. Since we do not know the values of L_v and B for our range of We, we can only calculate directly E_V using the energy balance for Teflon on gold. As this surface shows negligible charging effects, then $E_V = E_T - E_R - E_F$. Thus, we have all the necessary contributions of energy to calculate E_{ef} for Teflon on SiO_2 by energy balance.

Our calculations indicate that E_V increases with We and dominates over the other sources of energy dissipation [Fig. 7(a)], as suggested recently by Wang *et al.*[47] For instance, E_V can be up to 80% of the initial impact energy (at We = 82, $E_T \sim 6 \times 10^{-6}$ J). E_F remains constant as We increases. In fact, the variation of R_{max} at different We is less than ~0.9 mm. This is a quite low value to make a significant change in E_F. Similarly, the increase in We does not affect importantly E_{ef}. Although the contribution of E_{ef} is one order of magnitude lower than E_V, it is not negligible, but comparable to E_F. This implies that the influence of electrostatic forces in the retraction motion, indeed, exists. The work exerted by these forces on a fully retracted contact line is then

$$E_{ef} = 2F_{ef} R_{max}, \quad (10)$$

where F_{ef} is the average electrostatic force experienced on the drop rim. Our results reveal that varying We does not influence considerably F_{ef} [Fig. 7(b)]. At the first moments of retraction, the surface charge density is close to its highest value. With further retraction, more charge is deposited on the surface. This should increase the electrostatic force pulling the drop rim outward. However, the increase in charge is compensated with a larger retracted contact area. Therefore, the magnitude of the generated electrostatic forces appears independent of the further charge deposition on the surface induced by the increasing We.

2. After rebound

We calculated the average electrostatic force experienced by the primary drop from the taking off until the drop reaches h_{max}. For the calculation, we used conservation of energy for drop motion. When

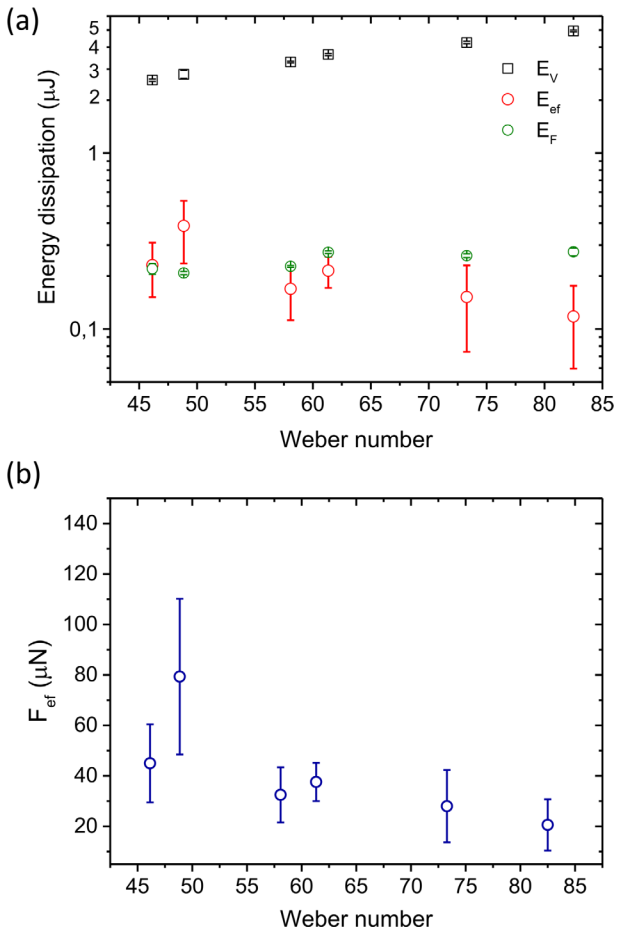

FIG. 7. (a) Sources of energy dissipation during the retraction motion: Viscous dissipation (E_V), energy dissipated by friction forces (E_F), and electrostatic forces (E_f) as a function of Weber number. (b) Average electrostatic force during the retraction motion as a function of a Weber number.

the drop bounces off, the total amount of energy, E_T, is equivalent to the contribution of the kinetic energy, E_k; potential energy, E_{p_1}; and the electric energy of the drop E_{Q1p}. At this point, the total energy should be equivalent to the potential energy E_{p_2} at the maximum rebounding height h_{max}, plus the contribution of the electric energy E_{Q2p} and the absolute value of the work done by the electrostatic force, E_{FE}

$$E_T = E_k + E_{p_1} + E_{Q1p} = E_{p_2} + E_{Q2p} + |E_{F_E}|, \quad (11)$$

$$E_T = \frac{1}{2} m v_{1p}^2 + mgh_{1p} + \frac{Q_p^2}{4\pi\varepsilon_0 h_{1p}} = mgh_{max} + \frac{Q_p^2}{4\pi\varepsilon_0 h_{max}} + |E_{F_E}|, \quad (12)$$

where g = 9.8 m/s^2 is the gravity acceleration. Furthermore, the drag force and damping forces due to the oscillations after rebound do not contribute to the energy dissipation. The drag force can be calculated by the equation: $F_D = \frac{1}{2} C_D \rho_a U^2 A$, where ρ_a is the density of the air, C_D is the drag coefficient (~0.52), U is the speed of the drop, and A is

its cross-sectional area. At We = 82, $F_D = 0.3\ \mu$N, which is 2 orders of magnitude smaller than the gravity force. The contribution of viscous dissipation in air should not be significant in comparison with the dissipation due to electrostatic forces, as explained previously.

An average electrostatic force F_E will exert a work on the primary drop of $|E_{FE}| = F_E(h_{max} - h_{1p})$. Therefore, F_E can be written as

$$F_E = \frac{mv_{1p}^2}{2(h_{max} - h_{1p})} - mg + \frac{Q_p^2}{4\pi\varepsilon_0 h_{1p} h_{max}}. \quad (13)$$

The calculations of F_E from Eq. (13) reveal that it is independent of *We* [Fig. 8(a)]. This result can be explained by how the drop charge and h_{max} vary with *We*. The electrostatic forces become weaker as longer is the distance between the drop and the surface. Then, these forces reach the maximum values at the first moments of rebound and the minimum at h_{max}. As *We* increases, there is an increment of both drop/surface charge and h_{max}. This should increase the average electrostatic force F_E mostly immediately after the rebound, which is compensated by the excess in h_{max}. As a result, F_E does not change significantly with *We*. Note that the magnitude of F_E is in good quantitative agreement with the values of electrostatic forces for sliding drops on the same surfaces.[21] The electrostatic forces are, in fact, significant and can be even higher than the gravitational force (40 μN) especially shortly after the rebound when the distance between drop and surfaces is smallest. Hence, the electrostatic forces are sufficient to decrease the maximum rebounding height.

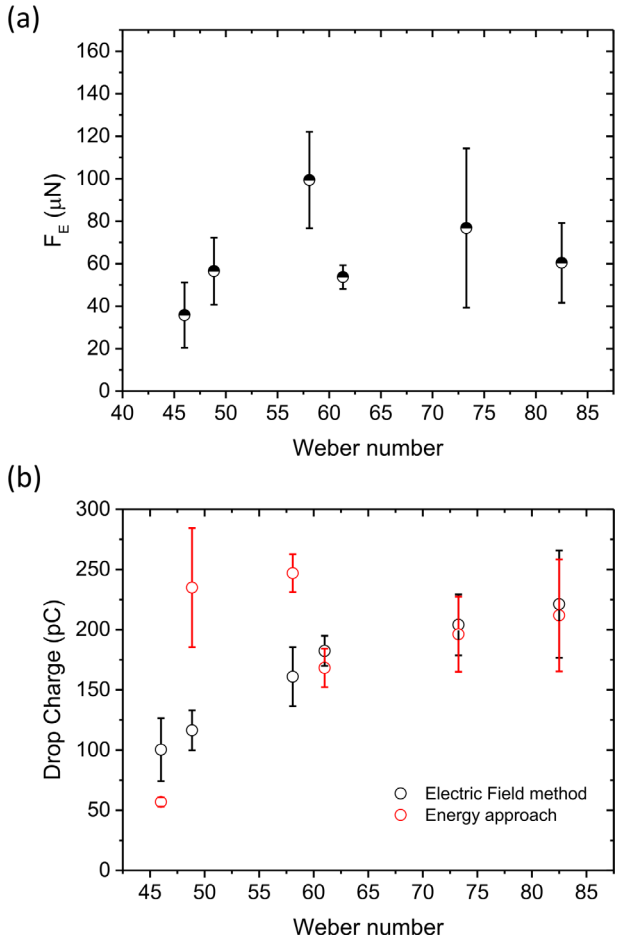

FIG. 8. (a) Average electrostatic force after the rebound acting on a primary drop vs Weber number. (b) Drop charge vs Weber number for the electric field method and the prediction using the energy approach for a primary drop.

Assuming net charges of equal magnitude and opposite sign on the surface and in the drop mass center after the rebound, the average electrostatic force can be represented by the Coulomb's law

$$F_E = \frac{kQ^2}{r^2}. \quad (14)$$

Here, k is the Coulomb constant and Q is the drop and surface charge. As we obtained the average electrostatic force from the work done on the drop, we considered $r = h_{max} - h_{1p}$. This means that E_{FE} can be rewritten as kQ^2/r, which is the average electric energy of a drop rebounding a distance r from the surface. Notably, our energy approach is also suitable to determine the charge of the rebounding drops. Replacing Eq. (14) with Eq. (13) leads to

$$E_k + E_{p1} - E_{p2} = \frac{Q^2}{4\pi\varepsilon_0}\beta, \quad (15)$$

with

$$\beta = \frac{1}{4\pi\varepsilon_0}\left[\frac{1}{(h_{max} - h_{1p})} + \frac{1}{h_{max}} + \frac{1}{h_{1p}}\right]. \quad (16)$$

The drop charge Q is then

$$Q = \sqrt{\beta^{-1}\left[\frac{1}{2}mv_{1p}^2 - mg(h_{max} - h_{1p})\right]}. \quad (17)$$

This new approach for determining drop charge calculation from the change in rebounding height gives comparable values as those measured by the electric field method [Fig. 8(b)]. Thus, the charge of drops rebounding from hydrophobic surfaces can be estimated by high-speed video imaging, without external electric fields or electronic devices for drop charge detection, if one can use a reference surface that does not lead to charging.

IV. DROP CHARGING ON SU-8 MICROPILLAR ARRAYS

We performed additional drop impact experiments on SU-8 micropillars surfaces because their effective contact area is well defined. This allows to show further evidence of the role of the effective contact area in the charge separation process. SU-8 micropillar surfaces are hydrophobic according to their wetting properties, but they behave like superhydrophobic surfaces since rebounding drops can remain in the Cassie–Baxter state. Although drops can also rebound after impacting on micropillar surfaces, the range of Weber numbers is restricted to $5 < We < 15$. Above this range, drops impale into the surface and cannot rebound completely. This means that drops penetrate into the space between the pillars, leading to the Cassie–Wenzel transition.[48] Here, part of the initial drop volume is left on the surface and secondary drops are ejected upon impact.

We observed positively charged drops deflected by electric fields upon impact on the micropillars [Fig. 9(a) (Multimedia view)].

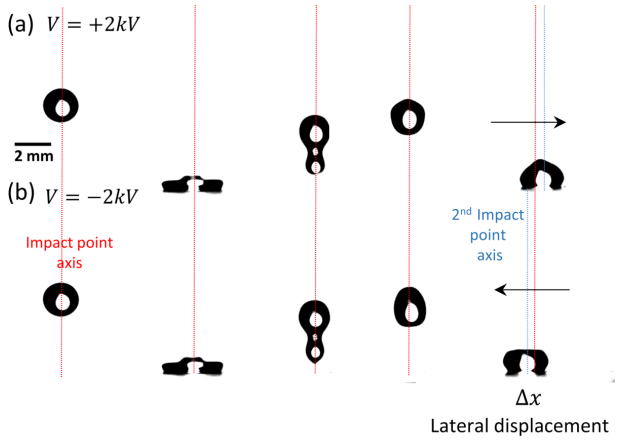

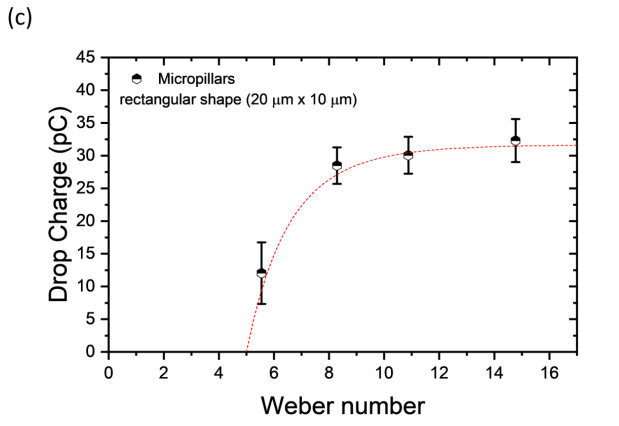

FIG. 9. (a) and (b) 4 μL drop rebounding from a SU-8 micropillar arrays surface ($We = 15$) when an electric field is applied from (a) left to right and (b) right to left. (c) Drop charge vs Weber number for a SU-8 micropillar surface. The red dotted line represents the fit of the theoretical model, with $\sigma_0 = 21\ \mu C/m^2$ and $\lambda_r = 0.49$ mm. Error bars represent the standard deviation of four measurements. Multimedia view: https://doi.org/10.1063/5.0130343.5

Experiments at different *We* showed that drop charge on micropillars saturates quickly at $We = 8$ [Fig. 9(b) (Multimedia view)], with charge values in the same order of magnitude as for superhydrophobic surfaces.[12] However, one would expect a more pronounced charging from a hydrophobic surface. We explain the charging on micropillars by the values of the effective liquid–solid contact area. In particular, we can calculate the area fraction of micropillars in contact with liquid by the equation $f = A_{pillar}/A_{LS} = 1/3$, where A_{pillar} is the area of the micropillar (50 μm^2) and A_{LS} is the projected liquid–solid contact area (150 μm^2). At $We = 15$, drops cover an apparent contact area of $A_{max} \sim 7$ mm^2. This leads to an effective area of $\sim$2.3 mm^2, which is comparable with the area fraction covered by a drop impacting a superhydrophobic surface.[12] Hence, the similarly reduced charge values of micropillars and superhydrophobic surfaces compared to hydrophobic surfaces are a consequence of their similar effective contact areas.

As micropillars exhibit the same scaling law between R_{max} and *We* (Fig. S8), we can fit Eq. (3) in Fig. 8. This leads to the fitting parameters $\sigma_0 = 21\ \mu C/m^2$ and $\lambda_r = 0.49$ mm for micropillars. The value of λ_r is quite similar to the value for superhydrophobic surfaces $\lambda_r = 0.6$ mm,[12] which is related to the fact that they exhibit similar saturation points. Since the magnitude of charge for micropillars is significantly smaller compared to Teflon on SiO_2, electrostatic force effects on the drop impact dynamics are strongly reduced as well and, therefore, hard to notice. The same applies for superhydrophobic surfaces.

V. CONCLUSIONS

We have shown that drops can rebound positively charged from hydrophobic surfaces. The amount of charge depends predominantly on the maximum spreading area covered by a drop. The charging can be up to two orders of magnitude higher than for superhydrophobic surfaces. Charging on micropillar surfaces leads to much lower charge when drops remain in the Cassie state. The decrease in charge is proportional to the decrease in the true liquid–solid contact area and leads to similar charge values as for other superhydrophobic surfaces.

Our experiments show that charge transfer can be suppressed by hydrophobic, high-permittivity surfaces. We observed that electrostatic forces influence drop impact dynamics in two ways. First, drop retraction motion. Charges deposited on the surface during retraction generate attractive forces between the rim of the positively charged drop and the charges left on the surface, reducing its retraction speed. Moreover, the unaltered drop spreading speed confirms that charge separation occurs in the retraction phase. Second, electrostatic forces reduce the maximum rebounding height that a drop can reach. When a drop rebounds, attractive electrostatic forces from the negatively charged surface decelerate the drop. Using conservation of energy, we calculated the average electrostatic force for both situations. These average forces depend only weakly on *We*. The increment in charge with *We* is compensated by the increasing spreading radius at the retraction phase and by the increasing maximum rebounding height after the rebound. The calculated average electrostatic forces can even surpass those due to gravity and are in good agreement with the ones resulting from the slide electrification phenomenon. The energy approach allows us to estimate the drop charge for a rebounding drop from a Teflon surface, by just recording its trajectory, without the need of external electric fields.

Charging of bouncing drops on hydrophobic surfaces arises as a new alternative for energy-harvesting applications based mainly on sliding drops. In addition, suppressing the drop charging with high-conductivity surfaces may be helpful in the fabrication of surfaces with better self-cleaning properties. It may also help prevent or enhance the sticking of drops on surfaces, which is crucial in applications such as printing or heat exchangers. Our findings are important for the description and analysis of drop impact by considering electrostatic forces as a new additional energy dissipation source.

SUPPLEMENTARY MATERIAL

See the supplementary material for further details of the experimental methods, uncertainties, and additional data.

ACKNOWLEDGMENTS

This project has received funding from the European Research Council (ERC) under the European Union's Horizon 2020 research and innovation program, Grant Agreement No. 883631, 'DynaMo' (H.-J. Butt, P.B.) and the Priority Program 2171 'Dynamic wetting

of flexible, adaptive and switchable surfaces' (Grant No. BE3286/6–1: X.L.). D.D. acknowledges the support from the Bilateral Agreement of the Doctoral scholarships DAAD/BECAS Chile, 2018 (No. 57395809). D.D. would like to thank D. Farías for helpful discussions.

AUTHOR DECLARATIONS

Conflict of Interest

The authors have no conflicts to disclose.

Author Contributions

Diego Ignacio Diaz: Conceptualization (equal); Formal analysis (equal); Writing – original draft (equal); Writing – review & editing (equal). **Xiaomei Li:** Investigation (equal); Methodology (equal); Writing – original draft (supporting). **Pravash Bista:** Investigation (equal); Methodology (equal). **Xiaoteng Zhou:** Formal analysis (equal); Methodology (equal); Software (equal). **Fahime Darvish:** Investigation (equal); Methodology (equal); Writing – original draft (supporting). **Hans-Jürgen Butt:** Conceptualization (equal); Supervision (lead); Writing – original draft (supporting). **Michael Kappl:** Conceptualization (equal); Supervision (equal); Writing – original draft (supporting).

DATA AVAILABILITY

The data that support the findings of this study are available within the article (and its supplementary material).

REFERENCES

[1]K. Yatsuzuka, Y. Mizuno, and K. Asano, "Electrification phenomena of pure water droplets dripping and sliding on a polymer surface," J. Electrostat. **32**, 157–171 (1994).
[2]L. Helseth and H. Wen, "Visualisation of charge dynamics when water droplets move off a hydrophobic surface," Eur. J. Phys. **38**, 055804 (2017).
[3]L. E. Helseth, "The influence of microscale surface roughness on water-droplet contact electrification," Langmuir **35**, 8268–8275 (2019).
[4]A. Shahzad, K. R. Wijewardhana, and J.-K. Song, "Contact electrification efficiency dependence on surface energy at the water-solid interface," Appl. Phys. Lett. **113**, 023901 (2018).
[5]A. Z. Stetten, D. S. Golovko, S. A. Weber, and H.-J. Butt, "Slide electrification: Charging of surfaces by moving water drops," Soft Matter **15**, 8667–8679 (2019).
[6]N. Miljkovic, D. J. Preston, R. Enright, and E. N. Wang, "Electrostatic charging of jumping droplets," Nat. Commun. **4**, 2517 (2013).
[7]P. Lenard, "Ueber die electricität der wasserfälle," Ann. Phys. **282**, 584–636 (1892).
[8]Z. Levin and P. V. Hobbs, "Splashing of water drops on solid and wetted surfaces: Hydrodynamics and charge separation," Philos. Trans. R. Soc. London, Ser. A **269**, 555–585 (1971).
[9]J. Thomson, "Xxxi. on the electricity of drops," London Edinburgh Dublin Philos. Mag. J. Sci. **37**, 341–358 (1894).
[10]D. Chate and A. Kamra, "Charge separation associated with splashing of water drops on solid surfaces," Atmos. Res. **29**, 115–128 (1993).
[11]H. Wu, N. Mendel, D. van den Ende, G. Zhou, and F. Mugele, "Energy harvesting from drops impacting onto charged surfaces," Phys. Rev. Lett. **125**, 078301 (2020).
[12]D. Díaz, D. Garcia-Gonzalez, P. Bista, S. A. L. Weber, H.-J. Butt, A. Stetten, and M. Kappl, "Charging of drops impacting onto superhydrophobic surfaces," Soft Matter **18**, 1628–1635 (2022).
[13]J. K. Beattie, "The intrinsic charge on hydrophobic microfluidic substrates," Lab Chip **6**, 1409–1411 (2006).
[14]V. Tandon, S. K. Bhagavatula, W. C. Nelson, and B. J. Kirby, "Zeta potential and electroosmotic mobility in microfluidic devices fabricated from hydrophobic polymers. I. The origins of charge," Electrophoresis **29**, 1092–1101 (2008).
[15]T. Preočanin, A. Selmani, P. Lindqvist-Reis, F. Heberling, N. Kallay, and J. Lützenkirchen, "Surface charge at teflon/aqueous solution of potassium chloride interfaces," Colloids Surf., A **412**, 120–128 (2012).
[16]C. Tian and Y. Shen, "Structure and charging of hydrophobic material/water interfaces studied by phase-sensitive sum-frequency vibrational spectroscopy," Proc. Natl. Acad. Sci. **106**, 15148–15153 (2009).
[17]S. Lin, L. Xu, A. C. Wang, and Z. L. Wang, "Quantifying electron-transfer in liquid-solid contact electrification and the formation of electric double-layer," Nat. Commun. **11**, 399 (2020).
[18]I. Langmuir, "Surface electrification due to the recession of aqueous solutions from hydrophobic surfaces," J. Am. Chem. Soc. **60**, 1190–1194 (1938).
[19]R. Digilov, "Charge-induced modification of contact angle: The secondary electrocapillary effect," Langmuir **16**, 6719–6723 (2000).
[20]Q. Sun, D. Wang, Y. Li, J. Zhang, S. Ye, J. Cui, L. Chen, Z. Wang, H.-J. Butt, D. Vollmer *et al.*, "Surface charge printing for programmed droplet transport," Nat. Mater. **18**, 936–941 (2019).
[21]X. Li, P. Bista, A. Z. Stetten, H. Bonart, M. T. Schür, S. Hardt, F. Bodziony, H. Marschall, A. Saal, X. Deng *et al.*, "Spontaneous charging affects the motion of sliding drops," Nat. Phys. **18**, 713–717 (2022).
[22]A. M. Duffin and R. J. Saykally, "Electrokinetic power generation from liquid water microjets," J. Phys. Chem. C **112**, 17018–17022 (2008).
[23]T. Krupenkin and J. A. Taylor, "Reverse electrowetting as a new approach to high-power energy harvesting," Nat. Commun. **2**, 448 (2011).
[24]Z. Yang, E. Halvorsen, and T. Dong, "Power generation from conductive droplet sliding on electret film," Appl. Phys. Lett. **100**, 213905 (2012).
[25]J. K. Moon, J. Jeong, D. Lee, and H. K. Pak, "Electrical power generation by mechanically modulating electrical double layers," Nat. Commun. **4**, 1487 (2013).
[26]Z.-H. Lin, G. Cheng, L. Lin, S. Lee, and Z. L. Wang, "Water–solid surface contact electrification and its use for harvesting liquid-wave energy," Angew. Chem. Int. Ed. **52**, 12545–12549 (2013).
[27]S.-H. Kwon, J. Park, W. K. Kim, Y. Yang, E. Lee, C. J. Han, S. Y. Park, J. Lee, and Y. S. Kim, "An effective energy harvesting method from a natural water motion active transducer," Energy Environ. Sci. **7**, 3279–3283 (2014).
[28]Y. Xie, D. Bos, L. J. De Vreede, H. L. De Boer, M.-J. van der Meulen, M. Versluis, A. J. Sprenkels, A. van den Berg, and J. C. Eijkel, "High-efficiency ballistic electrostatic generator using microdroplets," Nat. Commun. **5**, 3575 (2014).
[29]L. Zheng, Z.-H. Lin, G. Cheng, W. Wu, X. Wen, S. Lee, and Z. L. Wang, "Silicon-based hybrid cell for harvesting solar energy and raindrop electrostatic energy," Nano Energy **9**, 291–300 (2014).
[30]Q. Liang, X. Yan, Y. Gu, K. Zhang, M. Liang, S. Lu, X. Zheng, and Y. Zhang, "Highly transparent triboelectric nanogenerator for harvesting water-related energy reinforced by antireflection coating," Sci. Rep. **5**, 9080 (2015).
[31]L. Helseth and X. Guo, "Contact electrification and energy harvesting using periodically contacted and squeezed water droplets," Langmuir **31**, 3269–3276 (2015).
[32]L. Helseth, "Electrical energy harvesting from water droplets passing a hydrophobic polymer with a metal film on its back side," J. Electrostat. **81**, 64–70 (2016).
[33]W. Xu, H. Zheng, Y. Liu, X. Zhou, C. Zhang, Y. Song, X. Deng, M. Leung, Z. Yang, R. X. Xu *et al.*, "A droplet-based electricity generator with high instantaneous power density," Nature **578**, 392–396 (2020).
[34]L. Wang, Y. Song, W. Xu, W. Li, Y. Jin, S. Gao, S. Yang, C. Wu, S. Wang, and Z. Wang, "Harvesting energy from high-frequency impinging water droplets by a droplet-based electricity generator," EcoMat **3**, e12116 (2021).
[35]H. Chen, M. Marengo, and A. Amirfazli, "Drop impact onto semi-infinite solid surfaces with different wettabilities," Phys. Rev. Fluids **4**, 083601 (2019).
[36]C. Mundo, M. Sommerfeld, and C. Tropea, "On the modeling of liquid sprays impinging on surfaces," Atomization Sprays **8**, 625 (1998).
[37]I. V. Roisman, R. Rioboo, and C. Tropea, "Normal impact of a liquid drop on a dry surface: Model for spreading and receding," Proc. R. Soc. London, Ser. A **458**, 1411–1430 (2002).
[38]D. Richard, C. Clanet, and D. Quéré, "Contact time of a bouncing drop," Nature **417**, 811–811 (2002).

[39]C. Clanet, C. Béguin, D. Richard, and D. Quéré, "Maximal deformation of an impacting drop," J. Fluid Mech. **517**, 199–208 (2004).
[40]R. Rioboo, M. Voue, A. Vaillant, and J. De Coninck, "Drop impact on porous superhydrophobic polymer surfaces," Langmuir **24**, 14074–14077 (2008).
[41]K.-L. Pan, K.-C. Tseng, and C.-H. Wang, "Breakup of a droplet at high velocity impacting a solid surface," Exp. Fluids **48**, 143–156 (2010).
[42]K. Okumura, F. Chevy, D. Richard, D. Quéré, and C. Clanet, "Water spring: A model for bouncing drops," Europhys. Lett. **62**, 237 (2003).
[43]D. Bartolo, F. Bouamrirene, E. Verneuil, A. Buguin, P. Silberzan, and S. Moulinet, "Bouncing or sticky droplets: Impalement transitions on superhydrophobic micropatterned surfaces," Europhys. Lett. **74**, 299 (2006).
[44]P. K. Sharma and H. N. Dixit, "Energetics of a bouncing drop: Coefficient of restitution, bubble entrapment, and escape," Phys. Fluids **32**, 112107 (2020).
[45]H. N. Dalgamoni and X. Yong, "Numerical and theoretical modeling of droplet impact on spherical surfaces," Phys. Fluids **33**, 052112 (2021).
[46]X. Wang, Y.-B. Wang, L.-L. Jiao, Y.-R. Yang, and X.-D. Wang, "Energy analysis on rebound dynamics of two droplets impacting a superhydrophobic surface simultaneously," AIP Adv. **11**, 055007 (2021).
[47]Y. Wang, Y. Zhao, L. Sun, A. A. Mehrizi, S. Lin, J. Guo, and L. Chen, "Successive rebounds of impinging water droplets on superhydrophobic surfaces," Langmuir **38**, 3860–3867 (2022).
[48]M. Broom and G. R. Willmott, "Water drop impacts on regular micropillar arrays: The impact region," Phys. Fluids **34**, 017115 (2022).
[49]M. D. Sosa, M. L. Martínez Ricci, L. L. Missoni, D. H. Murgida, A. Cánneva, N. B. D'Accorso, and R. M. Negri, "Liquid–polymer triboelectricity: Chemical mechanisms in the contact electrification process," Soft Matter **16**, 7040–7051 (2020).
[50]A. M. Worthington and R. B. Clifton, "XXVIII. On the forms assumed by drops of liquids falling vertically on a horizontal plate," Proc. R. Soc. London **25**, 261–272 (1877).
[51]R. Zimmermann, U. Freudenberg, R. Schweiß, D. Küttner, and C. Werner, "Hydroxide and hydronium ion adsorption—A survey," Curr. Opin. Colloid Interface Sci. **15**, 196–202 (2010).
[52]D. Bartolo, C. Josserand, and D. Bonn, "Singular jets and bubbles in drop impact," Phys. Rev. Lett. **96**, 124501 (2006).
[53]D. Richard and D. Quéré, "Bouncing water drops," Europhys. Lett. **50**, 769–775 (2000).
[54]X. Li, S. Silge, A. Saal, G. Kircher, K. Koynov, R. Berger, and H.-J. Butt, "Adaptation of a styrene–acrylic acid copolymer surface to water," Langmuir **37**, 1571–1577 (2021).
[55]M. Pasandideh-Fard, Y. Qiao, S. Chandra, and J. Mostaghimi, "Capillary effects during droplet impact on a solid surface," Phys. Fluids **8**, 650–659 (1996).
[56]J. B. Lee, D. Derome, A. Dolatabadi, and J. Carmeliet, "Energy budget of liquid drop impact at maximum spreading: Numerical simulations and experiments," Langmuir **32**, 1279–1288 (2016).